

3D Hierarchical NiFe₂O₄ Nanosheets/Ni Foam Electrode Using for High Performance Supercapacitor

Junfu Chen¹, Fenglong Zhang^{1,2}, Zhenglong Li^{1*}, Xianghui Ren¹, Shanguo Han¹, Manxia Cai¹, Haitao Gao^{1,*}, Likun Li^{1,*}

¹ China-Ukraine Institute of Welding, Guangdong Academy of Sciences, Guangdong Provincial Key Laboratory of Advanced Welding Technology, Guangzhou, 510650, P. R. China

² Faculty of Intelligent Manufacturing, Wuyi University, Jiangmen, 529020, P. R. China

*E-mail: lizhl@gwi.gd.cn, gaoh@gti.gd.cn, lilk@gwi.gd.cn

Received: 7 May 2022 / Accepted: 25 June 2022 / Published: 7 August 2022

Herein, we have designed and synthesized a electrode made up of NiFe₂O₄ nanosheets grown on three-dimensional nickel foam (NiFe₂O₄/NF) via a facile hydrothermal method. As a pseudocapacitor, the as-prepared NiFe₂O₄/NF electrode exhibited a relatively high capacitance (975 F g⁻¹ at current density of 1 A g⁻¹), excellent cycle life (about 95% capacitance retention after 3000 charge-discharge cycles at 10 A g⁻¹) and good rate capability (74.6% capacitance retention from 1 to 10 A g⁻¹). This work not only shows a simple way to enhance high electrochemical performance, but also demonstrates that the prepared freestanding NiFe₂O₄/NF electrode could be a potential electrode material for high performance supercapacitors.

Keyword: Fe-Ni double oxides, nanosheets, nickel foam, supercapacitor

1. INTRODUCTION

Sustainable and renewable clean resources have attracted significant research attention due to the fast development of the worldwide economy, the persistent consumption of fossil fuels, the deepening crisis of environmental pollution, the rapid expansion market for mobile electronic devices[1-5]. Among numerous energy conversion and storage devices, supercapacitors have attracted great interest in the past decades due to the fast charging and discharging rate, high reliability, long cycle lifetime, and high-power density [6-10]. Supercapacitors, also called electrochemical capacitors (ECs), which have three main kinds of electrode materials, including carbonaceous materials [11], metal oxides/hydroxides [12,13], and conducting polymers [14]. However, due to the physical charge accumulation through the reversible adsorption/desorption of ions at the electrode/electrolyte interface, carbon-based electrode materials usually show low energy density. Consequently, metal oxides, hydroxides and conducting

polymers directly store charges during the reversible and fast faradaic redox reactions occurring on the surfaces, which produces relatively high energy density.

Recently, many transition metal oxides-based ECs have caused the extensive concerns, such as hydrous RuO_2 [15], Fe_2O_3 [16], Co_3O_4 [17], NiO [18,19], MnO_2 [20], V_2O_5 [21]. Interestingly, binary transition metal oxide materials have been attracting lots of attentions for the synergistic effect from the both metal ions, such as Co-Ni double oxides [22], Fe-Co double oxides [23], Mn-Ni double oxides [24], Mn-Fe double oxides [25] and Fe-Ni double oxides [26,27]. However, the electrochemical performance of those binary oxides also trapped due to their innate weakness such as low electroconductivity, strong tendency aggregation and limited effective active surface area. Consequently, to overcome these issues, scientists utilized a series of three-dimensional (3D) conductive architecture with high electrical conductivity to enhance the electrochemical activity. Thus, herein, we have designed and synthesized a series of NiFe_2O_4 nanosheets grown on 3D nickel foam ($\text{NiFe}_2\text{O}_4/\text{NF}$) via a facile hydrothermal method. Remarkably, the $\text{NiFe}_2\text{O}_4/\text{NF}$ electrode exhibited a relatively high capacitance (975 F g^{-1} at current density of 1 A g^{-1}), excellent cycle life (about 95% capacitance retention after 3000 cycles at 10 A g^{-1}) and good rate capability (74.6% capacitance retention from 1 to 10 A g^{-1}). This work not only shows a simple way to enhance high electrochemical performance, but also demonstrates that the $\text{NiFe}_2\text{O}_4/\text{NF}$ can be considered as an appealing efficient electrode for supercapacitor.

2. EXPERIMENTAL

2.1. Material synthesis

All chemicals are of analytical grade and used as received without further purification. The deionized water was used in all experiments. Commercial nickel foam (NF) with a thickness of 1.2 mm were cut into size of $2 \times 4 \text{ cm}^2$, and was cleaned by sonication in 1 M HCl solution, absolute ethanol and deionized water for 20 min to remove the surface oxide layer and oil stain. Then the wet NF was dried at $80 \text{ }^\circ\text{C}$ for 12 h. In a typical synthesis of $\text{NiFe}_2\text{O}_4/\text{NF}$ electrode, 0.139 g of $\text{FeSO}_4 \cdot 7\text{H}_2\text{O}$, 0.0727 g of $\text{Ni}(\text{NO}_3)_2 \cdot 6\text{H}_2\text{O}$ and 0.09 g of $\text{CO}(\text{NH}_2)_2$ were dissolved in 30 mL of deionized water by magnetic stirring. Then a piece of treated NF was impregnated into the solution, and the reaction was transferred into a 50 mL Teflon-lined stainless autoclave and maintained at $180 \text{ }^\circ\text{C}$ for 12 h. After natural cooling to room temperature, the product was washed with mixed liquids with deionized water and ethanol, and then dried at $60 \text{ }^\circ\text{C}$ for 12 h in vacuum oven, subsequently the Fe-Ni layered double hydroxide (FeNi-LDH) on the Ni foam were obtained. Finally, the $\text{NiFe}_2\text{O}_4/\text{NF}$ composites were achieved by annealing the above product in a muffle at $350 \text{ }^\circ\text{C}$ for 2 h with a heating rate of $2 \text{ }^\circ\text{C min}^{-1}$. The mass loading of NiFe_2O_4 is about 1.0 mg cm^{-2} . In addition, NiFe_2O_4 powder samples were also obtained by the same experimental conditions without adding the NF.

2.2. Material characterization and electrochemical measurements

The X-ray diffraction (XRD) patterns were recorded on an X-ray diffractometer (type HZG41BPC) with Cu $\text{K}\alpha$ irradiation source ($\lambda = 0.15418 \text{ nm}$) at a scan rate (2θ) of 0.05 os^{-1} . SEM images were observed with S4800 field emission scanning electron microscope (FESEM, Hitachi, Japan) on the voltage of 7.5 kV. EDX using an instrument equipped in the FESEM. X-ray photoelectron

spectroscopy (XPS) measurements were performed on a Kratos XSAM800 XPS system with Al K α source and a charge neutralizer, and all the binding energies were referenced to the C 1s peak at 284.8 eV of the surface adventitious carbon. TEM images were obtained with a JEM-2100F electron microscope (JEOL, Japan). The accelerating voltage and the applied current were 50 kV and 100 mA. The electrochemical properties of the prepared samples were investigated by cyclic voltammetry (CV), electrochemical impedance spectroscopy (EIS) and galvanostatic charge-discharge (GCD) measurements with an electrochemical workstation (CHI760E Instruments, Shanghai Chenhua Instrument Crop., Shanghai, China). The electrochemical behavior of the active materials was tested with three-electrode system in a 2 M KOH electrolyte at room temperature, where NiFe-LDHs/rGO acted as working electrode, an Ag/AgCl and a 1.5×1.5cm² Pt plate were used as the reference and counter electrode.

NiFe₂O₄/NF sample could be used directly as working electrode with 1×1 cm². For powder materials, to prepare the working electrodes, a mixture of active materials, acetylene black and polyvinylidene fluoride (mass ratio 8:1:1) was dispersed in N-Methyl pyrrolidone (NMP) solvent to obtain a slurry. After painting onto a clean nickel foam (1×1 cm²), the electrode was dried at 80 °C overnight. The mass loading of active materials for individual electrodes was about 1.0 mg cm⁻². The electrochemical characterization of individual electrode was tested with three-electrode system in 2 M KOH electrolyte at room temperature, where Ag/AgCl and a platinum foil were used as the reference and counter electrodes, respectively. Cyclic voltammetry (CV), electrochemical impedance spectroscopy (EIS) and galvanostatic charge/discharge (GCD) measurements were performed using an electrochemical workstation (CHI 760E Instruments, Shanghai Chenhua Instrument Crop., Shanghai, China).

3. RESULTS AND DISCUSSION

The morphology and microstructure of pure nickel foam and NiFe₂O₄/NF samples were observed by the field-emission scanning electron microscopy (FESEM). As shown in Fig. 1a, the pure Ni foam shows a three-dimensional porous framework structure with smooth surface. Correspondently, almost all the surface of NiFe₂O₄/NF sample (Fig. 1b) becomes rougher than the original Ni foam, implying that NiFe₂O₄ was uniformly deposited on the Ni foam. The magnified FESEM images (Fig. 1c and 1d) further indicate the sheet-like structure of NiFe₂O₄, and these thin nanosheets are interconnected and perpendicularly grown on the surface of Ni foam.

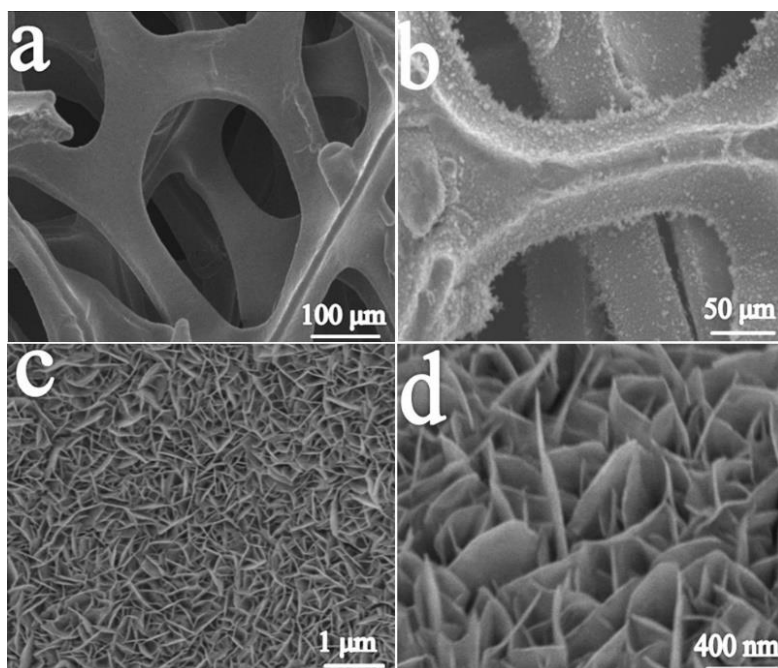


Figure 1. FESEM images of (a) pure nickel foam and (b-d) NiFe₂O₄/NF sample at different resolutions.

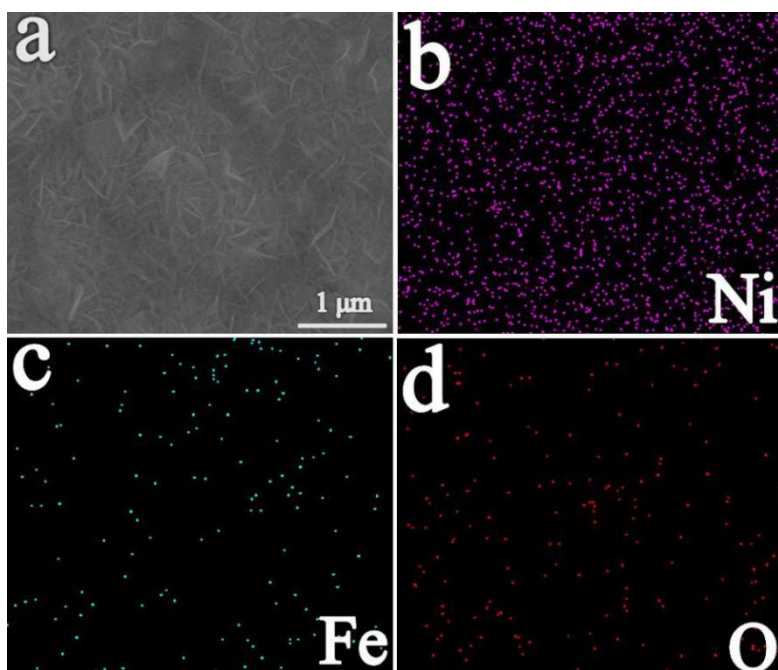


Figure 2. FESEM image and corresponding EDX elemental mappings of Ni, Fe and O from NiFe₂O₄/NF.

The FESEM and the corresponding elemental mapping images were shown in Fig. 2, the expected presence of Ni, Fe and O elements can be clearly observed. After strong ultrasonic vibration, the NiFe₂O₄ nanosheets were exfoliated from Ni foam and observed by TEM test. As shown in Fig. 3, the TEM images clearly indicate a thin plate-like structure of NiFe₂O₄. The SAED pattern (inset in Fig. 3b) obtained from a typical nanoplate shows a highly symmetrical dotted lattice, suggesting the single-crystalline characteristic of the sample. The HRTEM image of the nanosheet (Fig. 3c) shows a clear

lattice spacing of 0.25 nm, which can be attributed to the (311) plane of NiFe_2O_4 . Due to the low content of NiFe_2O_4 in $\text{NiFe}_2\text{O}_4/\text{NF}$ composite (1.0 mg cm^{-2}) and the strong diffraction peaks of Ni foam, there is no obvious characteristic peaks of NiFe_2O_4 can be detected from the XRD pattern of $\text{NiFe}_2\text{O}_4/\text{NF}$ hybrid samples. Consequently, the XRD patterns of pure NiFe_2O_4 and FeNi-LDH samples without Ni foam are presented in Fig. 3d. For FeNi-LDH sample, the sharp diffraction peaks appear at around 10.4° and 22.8° can be assigned to (003) and (006) planes, exhibiting the typical characteristics of layered double hydroxide materials. In addition, all the diffraction peaks can be indexed to FeNi-LDH (JCPDS card No. 40-0215) [28]. After annealing, all the strong diffraction peaks can be corresponded to NiFe_2O_4 with a cubic spinel crystalline structure (JCPDS card No. 10-0325), implying the full transformation of FeNi-LDH to NiFe_2O_4 .

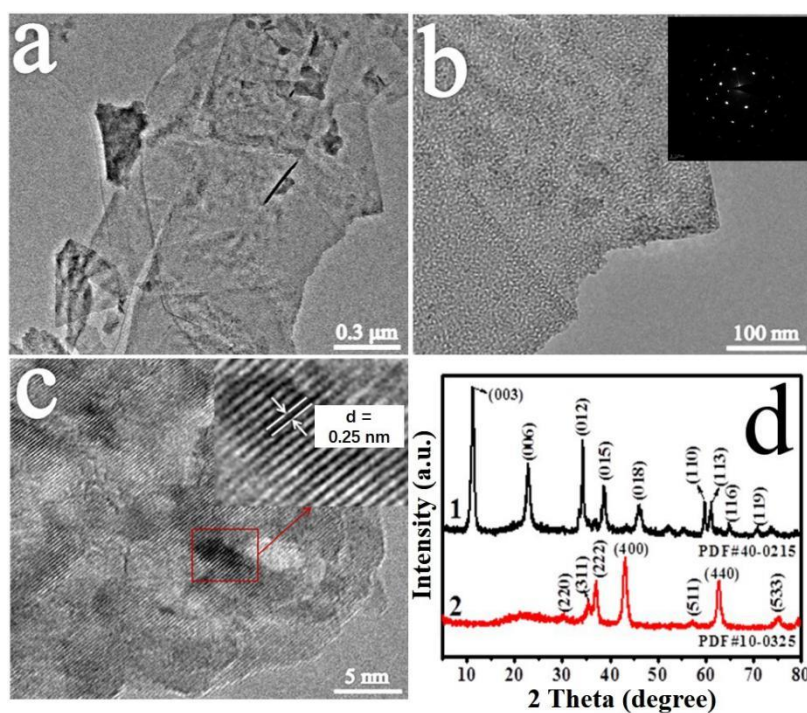


Figure 3. (a,b) TEM images and SAED pattern (inset) of NiFe_2O_4 nanosheets, (c) the high-resolution TEM image, the inset is magnification image of the square area, (d) XRD patterns of (1) FeNi-LDH and (2) NiFe_2O_4 samples.

X-ray photoelectron spectroscopy (XPS) was carried out to confirm the existence of NiFe_2O_4 and NF in the composites and to analyze their surface chemical states. In Fig. 4a, the survey spectrum of $\text{NiFe}_2\text{O}_4/\text{NF}$ sample confirms the existence of O, Fe, Ni and C elements, which further demonstrates the high purity of the product. The characteristic peaks observed in the O1s in Fig. 4b can be decomposed into three constituents at 530.1, 531.5 and 532.5 eV, assigning to metal-O bonds, metal-O-H and surface-adsorbed water molecules, respectively [29,30]. As shown in Fig. 4c, the XPS spectrum of Fe 2p showed binding energies of Fe $2p_{1/2}$ and Fe $2p_{3/2}$ at around 712.3 and 724.7 eV, respectively, suggesting the co-existence of Fe^{2+} and Fe^{3+} [31,32]. In addition, as can be seen in Fig. 3d, the fitting peaks at 855.7 and

873.3 eV can be attributed to Ni 2p_{3/2} and Ni 2p_{1/2} (the spin-energy separation is about 17.6 eV), while the peaks at 861.7 and 879.6 eV are two shake up satellite peaks, indicating the +2 oxidation state of Ni (Ni²⁺) in the sample [33].

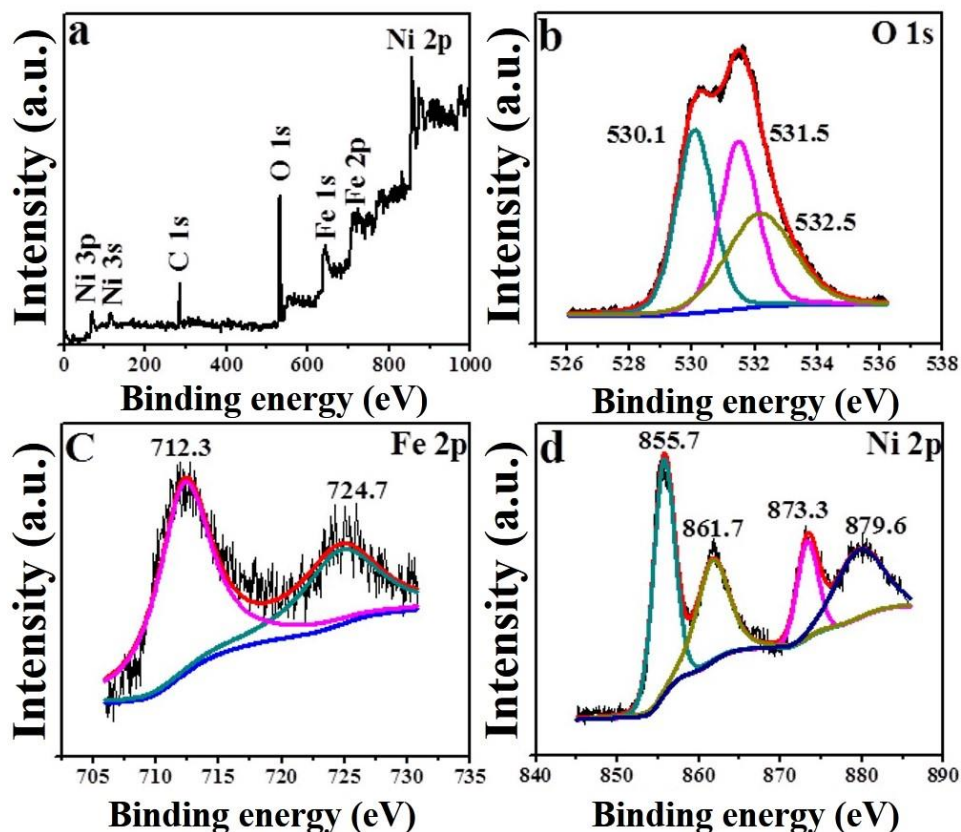


Figure 4. (a) Typical XPS survey spectrum of NiFe₂O₄/NF sample, and corresponding high-resolution XPS spectra of (b) O 1s, (c) Fe 2p and (d) Ni 2p.

The electrochemical activity of the as-prepared NiFe₂O₄/NF sample as a binder-free electrode was investigated by cyclic voltammetry (CV) and galvanostatic charge-discharge (GCD) technique in a traditional three-electrode system by using 2 M KOH as the aqueous electrolyte. The CV curves of NiFe₂O₄/NF sample in a potential window of 0 - 0.5 V (vs. Ag/AgCl) at scan rates ranging from 5 to 50 mV s⁻¹ are shown in Fig. 5a. Obviously, all the CV curves exhibit similar shape and show a set of intense redox peaks, revealing that the specific capacitance can be attributed to the reversible and fast electrochemical redox reactions [34,35]. Clearly, the peak potential shifts less than 100 mV with increasing the scan rates from 5 to 50 mV s⁻¹, reflecting that the working electrode has low polarization. The CV curves at the scan rate of 30 mV s⁻¹ for NiFe₂O₄/NF, NiFe₂O₄ and NF samples are shown in Fig. 5b. Clearly, the CV curve of pure NF is nearly a straight line, thus, the capacitance of NF can be neglected on this occasion. Importantly, the NiFe₂O₄/NF electrode shows a much larger integrated CV area than that of NiFe₂O₄ sample, indicating the better capacitive property [36]. These results directly reveal the

advantage of anchoring electrode materials on NF to be used as binder-free electrodes for capacitance improvement.

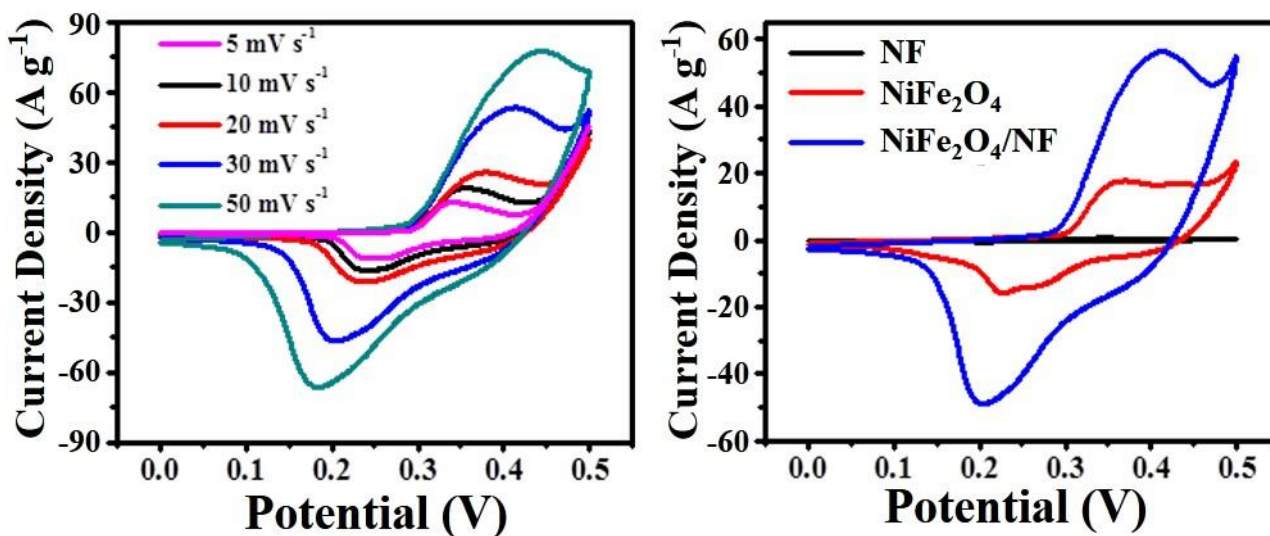


Figure 5. (a) CV curves of NiFe₂O₄/NF at different scan rates ranging from 5 to 50 mV s⁻¹; (b) CV curves of pure NF, NiFe₂O₄ powder and NiFe₂O₄/NF at a scan rate of 30 mV s⁻¹.

To further assess the specific capacitance of the NiFe₂O₄/NF electrode, GCD measurements were carried out at different current densities ranging from 1 to 10 A g⁻¹ with the potential window of 0 to 0.4 V. The C_s (specific capacitance) value of the electrode can be evaluated by the discharge time according to eq. (1):

$$C_s = \frac{I \times \Delta t}{m \times \Delta V} \quad (1)$$

where I , Δt , m , and ΔV represent discharge current, time, the mass of the active material in the electrode and potential window, respectively. As shown in Fig. 6b, the NiFe₂O₄/NF electrode exhibits a high specific capacitance of 975 F g⁻¹ at the low current density of 1 A g⁻¹ and maintained a capacitance of 727 F g⁻¹ at a high current density of 10 A g⁻¹. The retention ratio is about 74.5%, indicating the excellent rate capability. The high specific capacitance of the prepared NiFe₂O₄/NF electrode is superior or comparable to most of the recently reported spinel transition metal oxide-based electrode materials.

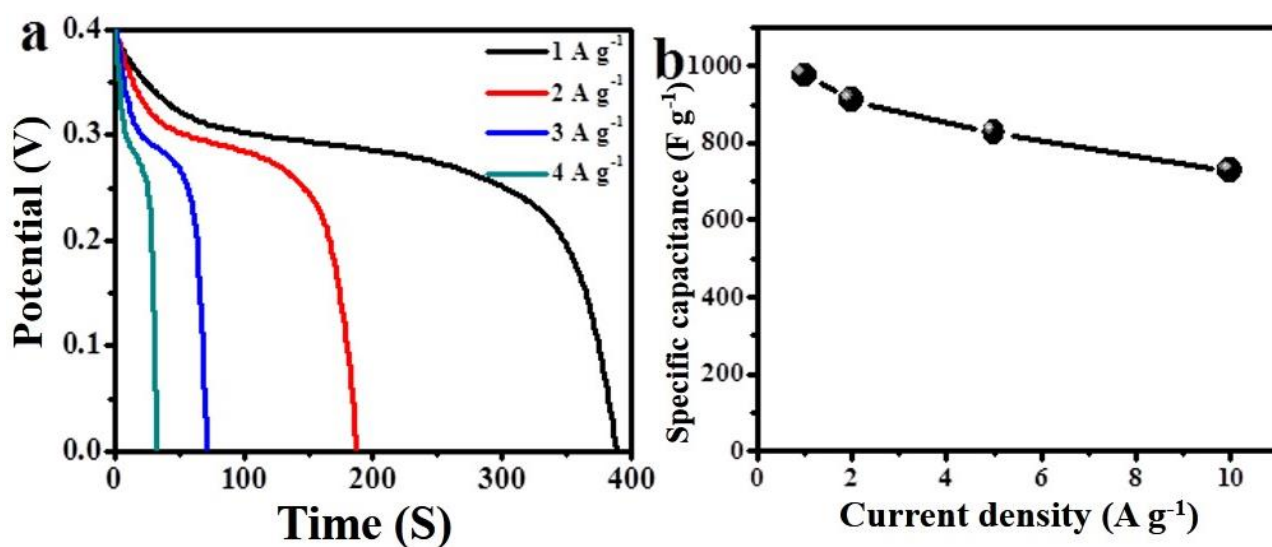


Figure 6. (a) Discharge profiles of NiFe₂O₄/NF at different current densities ranging from 1 to 4 A g⁻¹; (b) specific capacitance of NiFe₂O₄/NF at various current density.

To further clarify the transport kinetics for electrochemical reaction process, electrochemical impedance spectrum (EIS) test was carried out and the Nyquist plots of NiFe₂O₄/NF and NiFe₂O₄ are shown in Fig. 7a. Obviously, the Nyquist plot of NiFe₂O₄/NF electrode is almost linear, while the NiFe₂O₄ sample shows a quasi-semicircular arch at high frequencies and an oblique line at low frequencies. The smaller semicircle means a lower charge transfer resistance (R_{ct}) and a steeper slope illustrates a lower resistance of electrolyte ions [34]. These results clearly illustrated that the NiFe₂O₄/NF composite has a smaller R_{ct} and exhibits a nearly ideal capacitive behavior with fast electrolyte ion diffusion, resulting in fast charge transformation and high electrolyte accessibility, thus enhancing the specific capacitance. The cycling stability of the electrode is another important parameter for practical application of the supercapacitors, which precisely reflects the service performance, is also investigated in our study. Fig. 7b shows the cycling ability of as-synthesized NiFe₂O₄/NF electrode for 3000 cycles at current density of 10 A g⁻¹. Significantly, the specific capacitance of NiFe₂O₄/NF electrode decreases slightly with an outstanding retention of about 95% after 3000 cycles, suggesting the excellent stability for long time charge-discharge applications. Also, the calculated electrochemical results of the NiFe₂O₄/NF electrode are compared with previous reports (Table 1). The enhanced electrochemical performance of NiFe₂O₄/NF electrode can be attributed to the specific 3D Ni foam framework with the NiFe₂O₄ nanosheets vertically grown on the surface. The intimate contact between NiFe₂O₄ nanosheets and 3D Ni foam through the *in-situ* growth method and such unique hierarchical structure are benefit for the electrical conductivity and diffusion kinetics, thereby enhancing the specific capacitance.

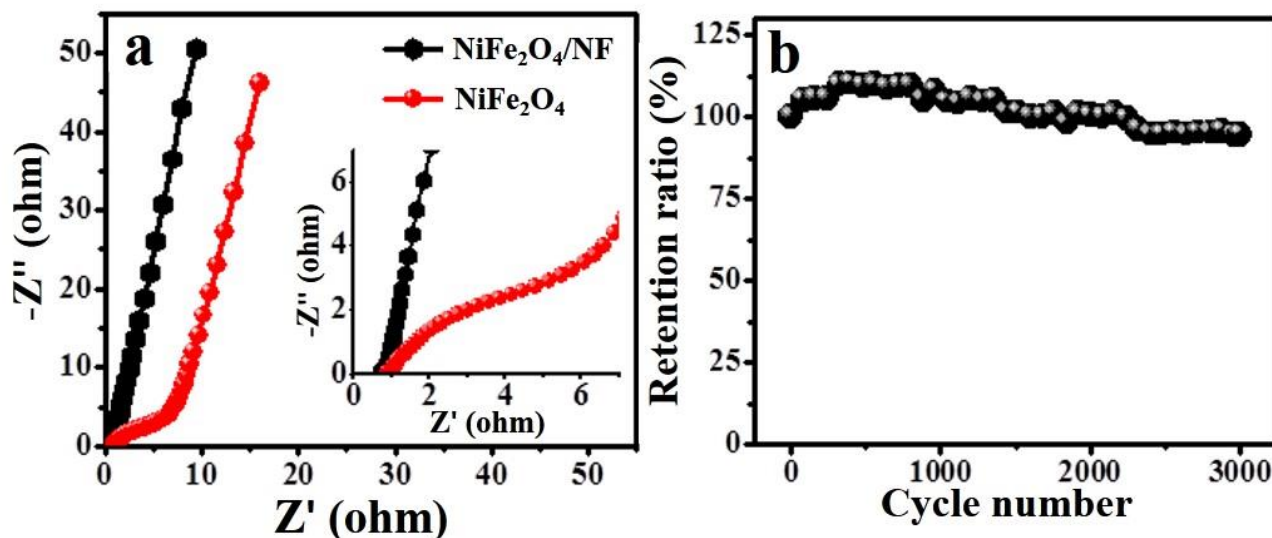


Figure 7. (a) Nyquist plots for NiFe₂O₄ and NiFe₂O₄/NF samples, the inset image shows the expanded plots at high frequency region, (b) Cycling stability of NiFe₂O₄/NF at a constant current density of 10 A g⁻¹.

Table 1. Comparison of the capacitance, cyclic stability, specific energy, and specific power of NiFe₂O₄/NF electrode with the relevant literature[2,12,13,26,27,37]

NO.	Material	Morphology	Specific Capacitance	Cyclic Stability	Ref.
1	NiFe ₂ O ₄	Sheet-like structure	240.9 F g ⁻¹ at 1 A g ⁻¹	128% after 2000 cycles	2
2	NiFe ₂ O ₄	Octahedral Nanocrystals	562.1 F g ⁻¹ at 4 A g ⁻¹	80.3% after 1500 cycles	12
3	NiFe ₂ O ₄ /MoS ₂	Nanoparticle on nanosheets	506 F g ⁻¹ at 1 A g ⁻¹	90.7% after 3000 cycles	13
4	NiFe ₂ O ₄ /Graphene	Nanosheets	464.1 F g ⁻¹ at 1 A g ⁻¹	140% after 5000 cycles	26
5	NiFe ₂ O ₄ /rGO	Nanoparticles	215.7 F g ⁻¹ at 0.5 A g ⁻¹	89.4% after 10000 cycles	27
6	NiFe ₂ O ₄	Mesh-like structure	833 F g ⁻¹ at 0.25 A g ⁻¹	73% after 700 cycles	37
7	NiFe ₂ O ₄ /NF	Sheet-like structure	975 F g ⁻¹ at 1 A g ⁻¹	95% after 3000 cycles	This Work

4. CONCLUSIONS

In summary, we have successfully developed a freestanding electrode made up of NiFe₂O₄ nanosheets grown on 3D nickel foam via a facile hydrothermal method. As a pseudocapacitor, the as-prepared NiFe₂O₄/NF electrode exhibited a relatively high capacitance of 975 F g⁻¹ at 1 A g⁻¹, excellent cycle life (about 95% capacitance retention after 3000 charge-discharge cycles at 10 A g⁻¹) and good rate capability (74.6% capacitance retention from 1 to 10 A g⁻¹). Such excellent capacitive behaviors of the NiFe₂O₄/NF electrode are mainly ascribed to the intimate contact between NiFe₂O₄ nanosheets and Ni foam and the unique hierarchical 3D structure. This work not only shows a simple way to enhance

high electrochemical performance but also shows that the freestanding NiFe₂O₄/NF electrode can be considered as an appealing candidate electrode for supercapacitors.

ACKNOWLEDGEMENTS

This work was supported by The GDAS' Project of Constructing Domestic First-class Research Institutions under Grant No. 2021GDASYL-20210103081. The GDAS' Projects of the Construction of the Domestic First-class Research Organization under Grant No. 2021GDASYL-20210103084. The National Key Research and Development Program of China (grant number 2020YFE0205300), Project of Guangdong Provincial Key Laboratory (grant number 2017B030314048).

DECLARATION OF COMPETING INTEREST

The authors declare that they have no known competing financial interests or personal relationships that could have appeared to influence the work reported in this paper.

References

1. V. V. Klimenko, S. V. Ratner and A. G. Tereshin, *Renewable Sustainable Energy Rev.*, 144 (2021) 111011.
2. X. Gao, W. Wang, J. Bi, Y. Chen, X. Hao, X. Sun and J. Zhang, *Electrochim. Acta*, 296 (2019) 181-189.
3. W. Tu, L. Zhang, Z. Zhou, X. Liu and Z. Fu, *Renewable Sustainable Energy Rev.*, 15 (2011) 856-860.
4. D. Mulvaney, R. M. Richards, M. D. Bazilian, E. Hensley, G. Clough and S. Sridhar, *Renewable Sustainable Energy Rev.*, 137 (2021) 110604.
5. C. H. Lim, S. Lim, S. H. Bing, W. P. Q. Ng, S. L. Ngan, W. D. Leong and H. L. Lam, *Renewable Sustainable Energy Rev.*, 135 (2021) 110223.
6. P. E. Lokhande, U. S. Chavan, S. Bhosale, A. Kalam and S. Deokar, *Flexible Supercapacitor Nanoarchitectonics*, 11 (2021) 277-314.
7. S. Chen, L. Wang and X. Hu, *Chem. Eng. J.*, 423 (2021) 130162.
8. H. Zhang, D. Yang, A. Lau, T. Ma, H. Lin and B. Jia, *Small*, 17 (2021) 2007311, 1-12.
9. S. Chen, L. Wang and X. Hu, *Chem. Eng. J.*, 423 (2021) 130162.
10. G. Yang, X. Zhao, F. Liao, Q. Cheng, L. Mao, H. Fa and L. Chen, *Sustainable Energy Fuels*, 5 (2021) 3039-3083.
11. L. H. Poudeh, I. Bertkas, H. Q. Ali, B. S. Okan and M. Yildiz, *Energy Technol.*, 8 (2020) 12, 2000714.
12. M. Hua, L. Xu, F. Cui, J. Lian, Y. Huang, J. Bao, J. Qiu, Y. Xu, H. Xu, Y. Zhao and H. Li, *J. Mater. Sci.*, 53 (2018) 7621-7636.
13. Y. Zhao, L. Xu, J. Yan, W. Yan, C. Wu, J. Lian, Y. Huang, J. Bao, J. Qiu, L. Xu, Y. Xu, H. Xu and H. Li, *J. Alloys Compd.*, 726 (2017) 608-617.
14. P. Naskar, A. Maiti, P. Chakraborty, D. Kundu, B. Biswas and A. Banerjee, *J. Mater. Chem. A*, 9 (2021) 4, 1970-2017.
15. B. Asbani, G. Buvat, J. Freixas, M. Huve, D. Troadec, P. Roussel, T. Brousse and C. Lethien, *Energy Storage Mater.*, 42 (2021) 259-267.
16. H. E. Lin, Y. Kubota, Y. Katayanagi, T. Kishi, T. Yano and N. Matsushita, *Electrochim. Acta*, 323 (2019) 134794.
17. R. K. Mishra, G. J. Choi, H. J. Choi, J. Singh, F. S. Mirsafi, H. G. Rubahn, Y. K. Mishra, S. H. Lee and J. S. Gwag, *Chem. Eng. J.*, 427 (2022) 131895.
18. H. T. Handal, W. A. A. Mohamed, A. A. Labib, S. A. Moustafa and A. A. Sery, *J. Energy Storage*,

- 44 (2021) 103321.
19. K. MadhusudanaRao, K. V. G. Raghavendra and S. S. Han, *J. Energy Storage*, 41 (2021) 102839.
 20. H. Zhang, H. Chai, A. Liu, W. Jia and Y. Cao, *Eur. J. Inorg. Chem.*, 2021 (2021) 43, 4489-4495.
 21. R. Velmurugan, P. Alagammai, M. Ulaganathan and B. Subramanian, *J. Mater. Chem. A*, 8 (2020) 45, 24148-24165.
 22. Y. Liu, C. Xiang, H. Chu, S. Qiu, J. McLeod, Z. She, F. Xu, L. Sun and Y. Zou, *J. Mater. Sci. Technol.*, 37 (2020) 135-142.
 23. C. Du, E. Han, L. Gao, L. Li, S. Qiao, L. Sun and J. Liu, *Ionics*, 26 (2020) 8, 4009-4018.
 24. S. Chen, S. Chandrasekaran, S. Cui and X. Zhang, *Inorg. Chem. Commun.*, 120 (2020) 108159.
 25. H. Gao, Y. Li, H. Zhao, J. Xiang and Y. Cao, *Electrochim. Acta*, 262 (2018) 241-251.
 26. X. Gao, J. Bi, W. Wang, H. Liu, Y. Chen, X. Hao, X. Sun and R. Liu, *J. Alloys Compd.*, 826 (2020) 154088.
 27. Y. Cai, W. Cao, P. He, Y. Zhang and M. Cao, *Mater. Res. Express*, 6 (2019) 105535.
 28. H. Li, F. Li, J. Yu and S. Cao, *Acta Phys. Chim. Sin.*, 37 (2021) 8, 2010073.
 29. M. Li, J. P. Cheng, F. Liu and X. B. Zhang, *Electrochim. Acta*, 178 (2015) 439-446.
 30. J. Yin, P. Zhou, L. An, L. Huang, C. Shao, J. Wang, H. Liu and P. Xi, *Nanoscale*, 8 (2016) 3, 1390-1400.
 31. T. Yamashita and P. Hayes, *Appl. Surf. Sci.*, 254 (2008) 8, 2441-2449.
 32. P. Singh, S. Mishra, A. Sahoo and S. Patra, *Sci. Rep.*, 11 (2021) 9035.
 33. S. Chen, J. Yu and J. Zhang, *J. CO2 Util.*, 24 (2018) 548-554.
 34. T. Liu, C. Jiang, B. Cheng, W. You and J. Yu, *J. Power Sources*, 359 (2017) 371-378.
 35. N. Wu, J. Low, T. Liu, J. Yu and S. Chao, *Appl. Surf. Sci.*, 413 (2017) 35-40.
 36. K. Xiao, T. Xiao, Y. Zhang, J. Xie, M. Cao, N. Li, T. Ouyang and Z. Liu, *Chem. Commun.*, 55 (2019) 17, 2513-2516.
 37. P. D. Patil, S. R. Shingte, V. C. Karade, J. H. Kim, T. D. Dongale, S. H. Mujawar, A. M. Patil and P. B. Patil, *J. Energy Storage*, 40 (2021) 102821.